Accepted Manuscript

Influence of the processing route on the properties of Ti(C,N)-Fe15Ni cermets

M. de Nicolás, H. Besharatloo, J.M. Wheeler, M. de Dios, P. Alvaredo, J.J. Roa, B. Ferrari, L. Llanes, E. Gordo

Please cite this article as: M. de Nicolás, H. Besharatloo, J.M. Wheeler, et al., Influence of the processing route on the properties of Ti(C,N)-Fe15Ni cermets, International Journal of Refractory Metals and Hard Materials, https://doi.org/10.1016/j.ijrmhm.2019.105046

INFLUENCE OF THE PROCESSING ROUTE ON THE PROPERTIES OF Ti(C,N)-Fe15Ni CERMETS

M. de Nicolás[1,*] mnicolas@ing.uc3m.es, H. Besharatloo[2,3], J. M. Wheeler[4], M. de Dios[1], P. Alvaredo[1], J. J. Roa[2,3], B. Ferrari[5], L. Llanes[2,3], E. Gordo[1]

[1]GTP – Department of Materials Science and Engineering, IAAB, Universidad Carlos III de Madrid, 28911 Leganés, Madrid, Spain

[2]CIEFMA – Department of Materials Science and Metallurgical Engineering, Universitat Politècnica de Catalunya - BarcelonaTech, 08019 Barcelona, Spain

[3]Centre for Research in Multiscale Engineering of Barcelona, Universitat Politècnica de Catalunya - BarcelonaTech, 08019 Barcelona, Spain

[4]Laboratory for Nanometallurgy, Department of Materials, ETH Zurich, Vladimir-Prelog-Weg 5, HCI G 503, 8093 Zürich, Switzerland

[5]Institute of Ceramic and Glass, CSIC, Kelsen, 5, 28049 Madrid, Spain

*Corresponding author.

Abstract

This study aims to understand the influence of powder preparation and processing steps on the microstructure and properties of Ti(C,N)-Fe15Ni cermets with 70 and 80 vol. % of ceramic phase. Two routes were used for powder preparation: (i) a colloidal approach, consisting of the preparation of stable aqueous suspensions of the powder particles and spray-drying to obtain easy-to-press granules, and (ii) conventional powder metallurgy route, consisting on wet ball milling of powders, with subsequent drying in rotary evaporator. The resultant powder mixtures were uniaxially pressed and sintered in high-vacuum at 1450 °C for 2 h. Sintered samples were characterized in terms of their density, porosity, microstructure (FESEM, image analysis), composition (EDX and XRD), small-scale hardness and sliding contact response by means of massive nanoindentation and nanoscratch testing. C content of the mixture powders was lower for conventional route, lost during milling. After sintering, all the materials, despite the processing route and composition, show C reduction, although that outflow is higher for the conventional powder metallurgy route, and more evident for the composition with higher binder content. As a result, COL samples exhibit a more homogeneous microstructural assemblage, higher small-scale hardness and mechanical integrity under sliding contact conditions. Compositions of materials must then be adjusted to adequate initial C addition with respect to the employed processing route, to account for the effects of the mixtures preparation stage.

1. Introduction

The cutting tool industry is actively searching for new materials as a substitute for traditional WC-Co cemented carbides, due to the inclusion of their constitutive elements in European and American lists of toxicity-related and critical raw materials [1,2]. Titanium carbonitride, Ti(C,N), arises as a feasible ceramic competitor, as it features high hardness, wear and corrosion resistance, and chemical stability [3,4]. Regarding the substitution of the cobalt-based binder, iron stands as an excellent candidate, having a relative low price and being non-hazardous for the human health [5]. Several investigations have claimed the advantage of using Fe instead of Co binders, for example, by improving the oxidation resistance of the final materials [6–9]. Nevertheless, the combination of Fe and Ti(C,N) has reported wettability problems [10], which directly translates into poor sinterability when processed by powder metallurgy.

Avoiding the addition of secondary carbides that could improve above sintering issue [11,12], another strategy to overcome lack of wettability for Fe-Ti(C,N) system is related to addition of binder alloying elements. Nickel has demonstrated throughout the years excellent capability to attain homogeneous and dense sintered hard materials [13–15]. Previous investigations demonstrated that introducing 15 wt. % of nickel as alloying element in the binder phase can improve binder-ceramic wettability, and lead to cermets with final properties comparable to some cemented carbides [10,16]. However, these materials are very sensitive to the processing route [17,18].

Following this, the present study aims to understand the influence of the powder preparation and processing steps in the microstructure and properties of Ti(C,N)-Fe15Ni cermets, using two ceramic contents: 70 and 80 vol. %. In doing so, extra carbon (C) was added to enhance the sinterability of the materials, as it is an element known to lower the solidus and liquidus temperatures of Fe [10,19]. Two routes were used for powder preparation:

- Colloidal (COL) route – consisting of the preparation of stable aqueous suspensions of the ceramic-metal powder particles and spray-drying to obtain easy-to-press granules, with a characteristic raspberry shape.

- Conventional powder metallurgy route (CPM) – entailing the ball milling of the metallic and ceramic powders.

Resulting powder mixtures were uniaxially pressed and sintered in high-vacuum furnace. The final sintered samples were characterized in terms of their density, microstructure, composition, nanohardness and sliding contact response at small length scale. The final objective was to reveal the influence of the processing route in the C content of powders and sintered samples, a parameter that directly influences the final properties.

2. Experimental procedure

The compositions used in this investigation are detailed in **Table 1**, correlating the volume of ceramic/metallic phases employed with reference-like WC-Co cemented carbide grades (Co wt. %). For both material configurations, 0.5 wt. % of extra carbon, with respect to the metallic binder content, was added.

Elemental powders were mixed and prepared following colloidal and conventional powder metallurgy routes, respectively. In the COL route, stable aqueous suspensions of the ceramic and metallic materials were prepared. De-ionized water was used as the solvent, modifying its pH to 10-11 with Tetramethylammonium hydroxide (TMAH), to ensure the chemical stability of the particles. Moreover, polyethylenimine (PEI, 0.4 wt. %) was added to ensure the colloidal stability of the suspensions and avoid surface oxidation, while polyvinyl alcohol (PVA, 2 wt. %) was added to favour granulation by spray-drying and achieve the final spherical shape of the agglomerates. Ceramic and metallic slurries were separately prepared and milled for 1 h at 50 rpm with silicon nitride (Si_3N_4) and nylon balls, respectively. The complete procedure is described in more detail in Ref. [17].

For the CPM route, the elemental powders were ball-milled in a tumbler and wet medium (isopropyl alcohol, 2-propanol) at 120 rpm during 24 h. Stainless steel vessel and balls were used, with a Ball-to-Powder Ratio (BPR) of 10:1. Polyethylene glycol (PEG) was added in a 2 wt. % to improve their compressibility. Then, the suspensions were dried in a rotary evaporator. **Figure 1** schematically illustrates a summary of the processing steps followed in each route.

The morphology of the obtained ceramic-metallic mixtures after each processing route was inspected by means of Scanning Electron Microscopy (SEM, XL-30 Philips). **Figure 2** shows the different appearance of the powders processed by COL and CPM routes, in backscattered electron (BSE) mode, for 70TiCN and 80TiCN compositions.

Carbon and oxygen contents of the mixture powders were measured using LECO CS-200 and TC-500 units, respectively. Then, they were pressed uniaxially at 600 MPa into 16 mm-diameter discs. The geometric or dimensional green relative density was estimated in terms of the theoretical density for each ceramic volume percent, calculated using the rule of mixtures.

Sintering of green samples was performed in a high-vacuum furnace (10^{-5} mbar), following the cycle: 800 °C – 30 min, 1450 °C – 2 h, with heating/cooling ramps of 5 °C/min. The density of sintered samples was measured both dimensionally and using an Accupyc He Multipycnometer (Micrometrics, USA). From the geometric and pycnometric sintered density values ($\rho_{geometric}$ and $\rho_{pycnometric}$, respectively), the total, closed and open porosities (P_{total}, P_{closed} and P_{open}, respectively) could be calculated [20]. The following equations were used:

$$P_{total} \, (\%) = 100 - \rho_{geometric} \tag{1}$$

$$P_{closed} \, (\%) = 100 - \rho_{pycnometric} \tag{2}$$

$$P_{open} \, (\%) = P_{total} - P_{closed} \tag{3}$$

Carbon content was also measured with LECO CS-200, to calculate the C lost during the sintering stage. The microstructure of the samples was studied by SEM (Phenom XL Desktop, PhenomWorld). Image analysis was employed to (1) quantify the ceramic/metallic phases in each material, (2) measure the binder mean free path of each material, employing the line interception method. Five images per sample type were evaluated with the software *ImageJ*. Composition of the samples was estimated by X-Ray Diffraction (XRD, Siemens-Bruker D8 Advance Diffractometer, Germany), performed using Cu-Kα radiation ($\lambda = 1.540598$ Å), and Energy Dispersive X-ray analysis (EDX), using SEM (XL-30 Philips, Netherlands). For the latter technique, five intrinsic-phase analysis were conducted, extracting the mean element content for each region (ceramic and binder). Considering the semi-quantitative nature of EDX data, it should be underlined that analysis done and ideas commented are based on sound trends, expected to be valid independent of the quantitative accuracy of the measured data.

Intrinsic hardness measurements, at the microstructural length scale, were performed to assess the hardness of each constitutive phase: ceramic, metallic and a composite-like one (corresponding to imprints probing regions including phase boundaries). A Berkovich diamond tip and a maximum load of 10 mN (iNano, KLA) were employed. A large number of imprints (40,000), with a lateral spacing of 1 μm, was performed for each material type. Histograms were extracted from the results of the massive nanoindentation testing and hardness estimation following the Oliver and Pharr method [21,22]. Subsequent statistical analysis, with Ulm and Constantinides methodology [23,24], was employed to extract the intrinsic hardness values of the tested samples, adjusting the data to Gaussian-distribution curves by the deconvolution of the Cumulative Distribution Function (CDF).

Moreover, a Nanoindenter XP (MTS) unit, also featuring a diamond Berkovich indenter, was used to measure the hardness of the materials and relate it to the small-scale hardness measured for the two-phase region including ceramic/metal interface boundaries. The system is equipped with a Continuous Stiffness Measurement (CSM) module performed to a target displacement of

2000 nm penetration depth (h), or until reaching the maximum applied load, 650 mN. An array of 9 indentations (3 by 3), with a separation of 50 μm between imprints, was performed. Nanoscratch, or sliding contact, tests were also performed with this equipment and tip on the cross-section of the polished samples. These were conducted by applying a constant load and velocity of 10 mN and 10 μm/s, respectively. Three scans per sample type were performed and residual scratches were observed by SEM (Phenom XL Desktop, PhenomWorld) [11].

3. Results and discussion

3.1. Carbon content

Table 2 collects the C content measurements of the cermet powders after COL and CPM processing, as well as that of resultant samples after the sintering process. First, it is noticeable that CPM mixture powders contain less C than colloidal ones for both compositions, a difference that is slightly lower for 80TiCN composition. A hypothesis for this C reduction is the reaction of this element with oxygen or its adhesion to the mill vessel and balls during the 24 h tumbling milling. Moreover, two different binders (PVA and PEG) were used for COL and CPM powders processing, but also colloidal powders contain an extra 0.4 wt. % of polymer (PEI) compared to CPM ones. Differences in the use of additives may also influence this higher C content for the former route. After sintering, all the materials, despite the processing route and composition, show C loss, although that outflow is higher for the conventional powder metallurgy route, and more evident for the composition with higher binder content (70TiCN).

Additionally, the oxygen content of the powder mixtures was also measured. As listed in **Table 3**, CPM powders contained more quantity of this element, which explains the higher C loss during the sintering cycle. Carbon would combine with oxygen present in the green samples, to form CO which is outgassed during the sintering stage [25,26], a reducing characteristic of carbon.

3.2. Density, microstructure image analysis and EDX

The green and sintered relative densities of the studied materials are collected in **Table 4**. This demonstrates that the CPM route achieves higher densities. It is worth noting that the closed porosity is higher for the colloidal samples, and that the materials with higher metal content exhibit an increase in their open porosity values.

Nevertheless, the opposite result was observed when examining the microstructures of the studied materials. SEM micrographs of 70TiCN and 80TiCN sintered samples, processed by COL and CPM routes, are displayed in **Figure 3**. For the colloidal route (left), a homogeneous carbide distribution can be appreciated, where the FeNi binder embeds and sustains the ceramic structure. Some small voids inside certain carbide particles can be discerned, which may correspond to incomplete carbide-carbide sintering. On the other hand, the CPM sample (right) shows a slightly different microstructure, with some carbide agglomeration and a larger number of voids between carbide particles. These features may indicate incomplete sintering of the samples [17]. This finding could be rationalized by a deficiency of C in CPM powders, as compared to COL powders, since C is an element known to enhance the densification phenomena by lowering solidus and liquidus temperatures [10,19]. Lack of C in the colloidal route leads to the similar microstructural features in Fe15Ni-Ti(C,N) cermets using 70, 80 and 85 vol. % of ceramic phase, as recently reported by the authors of this study [27], which confirms this hypothesis.

Moreover, a higher content of binder phase was determined in CPM samples. Image analysis results, collected in **Table 5**, confirm this fact: CPM samples contain more metal than the theoretical value for both compositions. This is also supported by the higher value of the mean free path in these materials. It is believed that part of the extra metal could have been gained during the milling process, collecting stainless-steel from the vessel and balls [28,29]. Another

hypothesis is that ceramic particles in CPM route partially dissolved during the sintering process but did not completely re-precipitate due to the lack of C [19]. Previous investigations have demonstrated the decisive role of this element in the dissolution-reprecipitation phenomena of Ti(C,N) carbides, particularly in terms of core-rim cermet structures [19,30]. Image analysis also reveals that COL samples show a lower binder content than the theoretical, which is essentially lost during sintering due to the vaporization of its composing elements [17].

Table 6 shows EDX intrinsic analysis of the different samples, displaying the results in wt. % for the binder phase and at. % for Ti(C,N). Fe/Ni ratio for the four material types is lower than the theoretical value (5.67), which means that Fe is lost during the sintering process. C/N ratio in the ceramic phase is lower than 1 for the four materials, with 80-COL being the material with a closer value to the theoretical. This implies that the Ti(C,N) phase of the four materials loses some C. It can be appreciated that CPM samples attain Fe/Ni and C/N ratios lower than COL ones for the same ceramic fraction. This result suggests the hypothesis that C migrates from the ceramic to the binder phase during solution-reprecipitation of carbides occurring in the sintering stage. Higher C migration may be experienced in CPM route to compensate lack of C of the powders. An increase of C concentration in the binder phase, as is the case of COL samples, may be promoting stabilization of Fe/Ni ratio by influencing the binder vapour pressure. Moreover, some Cr (~ 1-2 wt. %) could be measured in CPM route, not included in **Table 6** analysis for comparison purposes between the two processing routes. This small Cr content confirms slight contamination during the milling procedure from stainless steel of the vessel and balls.

3.3. Intrinsic and composite hardness tests

Figure 4 displays the type of histograms obtained after massive nanoindentation testing and hardness estimation. **Table 7** collects intrinsic hardness results for the studied processing routes

and compositions, extracted from mean values of the Gaussian CDF-adjusted curves from histograms. From these results, it appears that Ti(C,N) maintains its properties independently of the processing route employed or binder content. Moreover, the CPM binder phase is shown to be softer than in COL samples, and a similar result is observed for the composite hardness, especially in the 70TiCN sample, which exhibited the lowest C content of the four cases examined. This fact may be related to the influence of carbon in ceramic-metallic boundary region properties [19,30], achieved during the solution-reprecipitation of carbides during the sintering stage, as stated in the microstructural analysis (Section 3.2). A higher quantity of C dissolved in the metallic binder may contribute to harden this phase by solid-solution phenomena [17]. Additionally, the relatively superior hardness of the binder phase for COL samples may be also related to carbide constraining effects, as these samples haver a higher ceramic volume than CPM ones [31,32].

Intrinsic composite hardness coincides with Berkovich composite hardness values displayed in the plots of **Figure 5**, showing good agreement between results from the two nanoindentation systems employed. In these graphs, from 0 to 800 nm, the obtained hardness values fluctuate due to surface and tip effects, stabilizing and achieving an asymptote that shows the actual composite hardness value of each material.

3.4. Nanoscratch tests

Figure 6 collects the SEM images of the surface damage scenarios induced by the scratches of the sliding contact tests performed on COL/CPM 70TiCN and 80TiCN samples. Ductile binder deformation (A), detachment (B) and no-detachment (C) occurring at the ceramic-metal interface have been pointed out. As it can be appreciated, for the same volume of ceramic content, CPM samples show a more ductile response of the binder phase, with stacking of

planes, in consonance with the lower nanohardness results for this phase and processing route (**Table 7**). Moreover, there also seems to be more detachment at the ceramic-metal interface for both compositions in this processing route. This would suggest a lower mechanical integrity in this region [11], compared to colloidal samples, which is consistent with composite hardness findings (**Table 7** and **Figure 5**).

3.5. XRD analysis

X-Ray diffractograms for CPM/COL 70TiCN and 80TiCN compositions are shown in **Figure 7**. Firstly, it is worth noting that CPM samples show more intense binder peaks, as these samples contain a higher quantity of metal phase, compared to colloidal samples (**Table 5**). For the lowest carbide content samples, higher-intensity binder peaks were observed in comparison to 80TiCN samples, a logical result due to the higher metal content of this composition. However, the most interesting finding was the composition of the binder phase: COL shows an austenitic-ferritic structure, whereas CPM reveals that its metal constituent is exclusively ferritic. It is believed that the dissimilar crystallographic structure of the metal for each route may explain the differences in hardness and sliding contact response observed for the binder, depending on the processing route. Future characterization techniques, like TEM, will be implemented to gather more information about the effective influence of interstitial elements (like C or N) on the small-scale mechanical properties of the metallic phase.

4. Conclusions

In this investigation, Fe15Ni-TiCN cermets were manufactured, employing two processing routes – colloidal (COL) and conventional powder metallurgy (CPM) – and two compositions, 70 and 80 vol. % of ceramic phase. The following conclusions could be drawn:

- For the same ceramic/metal composition and carbon addition, it could be stated that CPM powder mixtures lost C during milling, due to reaction with oxygen and adhesion to milling balls/vessel.

- Sintered materials showed C loss, despite the processing route and composition. A higher outflow was observed for CPM route, more evident for the composition with higher binder content.

- C deficiency translates into poorer densification during sintering, as well as diminished mechanical properties in regions containing ceramic-metal phase boundaries. The latter is evidenced from results of nanoindentation and nanoscratch tests.

- XRD analysis of sintered samples showed the presence of austenitic-ferritic structure for COL route, whereas ferrite was the main binder phase in CPM samples. This different crystal formation may be related to binder hardness and sliding contact response. Future work will study the influence of interstitial elements present in the binder, like C or N.

- Overall, it could be concluded that initial powder composition, regarding C addition, must be tailored for each processing route, in order to account for the effects exerted by powder processing.

Acknowledgements

References

[1]   US National Toxicology Program (NTP), (n.d.). https://ntp.niehs.nih.gov/ (accessed April 1, 2019).

[2]   EU Registration, Evaluation, Authorisation and Restriction of Chemical substances (REACH) programme, (n.d.). https://ec.europa.eu/growth/sectors/chemicals/reach_en (accessed April 1, 2019).

[3]   Y. Peng, H. Miao, Z. Peng, Development of TiCN-based cermets: Mechanical properties and wear mechanism, Int. J. Refract. Met. Hard Mater. 39 (2013) 78–89. doi:10.1016/j.ijrmhm.2012.07.001.

[4]   S. Norgren, J. Garcia, A. Blomqvist, L. Yin, Trends in the P/M hard metal industry, Int. J. Refract. Met. Hard Mater. 48 (2015) 31–45. doi:10.1016/j.ijrmhm.2014.07.007.

[5]   J.A. Canteli, J.L. Cantero, N.C. Marín, B. Gómez, E. Gordo, M.H. Miguélez, Journal of Materials Processing Technology Cutting performance of TiCN – HSS cermet in dry machining, 210 (2010) 122–128. doi:10.1016/j.jmatprotec.2009.08.003.

[6]   B. Wittmann, W.-D. Schubert, B. Lux, WC grain growth and grain growth inhibition in nickel and iron binder hardmetals, Int. J. Refract. Met. Hard Mater. 20 (2002) 51–60. doi:10.1016/S0263-4368(01)00070-1.

[7]   B.J. Marques, C.M. Fernandes, A.M.R. Senos, Sintering, microstructure and properties of WC-AISI304 powder composites, J. Alloys Compd. 562 (2013) 164–170. doi:10.1016/j.jallcom.2013.02.013.

[8]   R. Furushima, K. Katou, K. Shimojima, H. Hosokawa, A. Matsumoto, Control of WC grain sizes and mechanical properties in WC-FeAl composite fabricated from vacuum sintering technique, Int. J. Refract. Met. Hard Mater. 50 (2015) 16–22. doi:10.1016/j.ijrmhm.2014.11.007.

[9]   O.J. Ojo-Kupoluyi, S.M. Tahir, B.T.H.T. Baharudin, M.A.A. Hanim, M.S. Anuar, Mechanical properties of WC-based hardmetals bonded with iron alloys – a review, Mater. Sci. Technol. 33 (2017) 507–517. doi:10.1080/02670836.2016.1186929.

[10]   P. Alvaredo, M. Dios, B. Ferrari, E. Gordo, Understanding of wetting and solubility

behavior of Fe binder on Ti(C,N) cermets, J. Alloys Compd. 770 (2019) 17–25. doi:10.1016/j.jallcom.2018.07.243.

[11] P. Alvaredo, J.J. Roa, E. Jiménez-Pique, L. Llanes, E. Gordo, Characterization of interfaces between TiCN and iron-base binders, Int. J. Refract. Met. Hard Mater. 63 (2017) 32–37. doi:10.1016/j.ijrmhm.2016.08.010.

[12] J. García, V.C. Ciprés, A. Blomqvist, B. Kaplan, Cemented carbide microstructures: A review, Int. J. Refract. Met. Hard Mater. 80 (2018) 40–68. doi:10.1016/j.ijrmhm.2018.12.004.

[13] V.A. Tracey, Nickel in Hardmetals, Refract. Met. Hard Mater. 11 (1992) 137–149. doi:10.1016/0263-4368(92)90056-8.

[14] J.M. Córdoba, E. Chicardi, F.J. Gotor, Liquid-phase sintering of Ti(C,N)-based cermets. The effects of binder nature and content on the solubility and wettability of hard ceramic phases, J. Alloys Compd. 559 (2013) 34–38. doi:10.1016/j.jallcom.2013.01.046.

[15] W.D. Schubert, M. Fugger, B. Wittmann, R. Useldinger, Aspects of sintering of cemented carbides with Fe-based binders, Int. J. Refract. Met. Hard Mater. 49 (2015) 110–123. doi:10.1016/j.ijrmhm.2014.07.028.

[16] H. Besharatloo, J.. Roa, M. de Dios, A. Mateo, B.Ferrari, E.Gordo, L. Llanes, Micromechanics of Ti(C,N)-FeNi composites: Statistical analysis and flow stress determination for the FeNiC binder, in: Euro PM 2017 Congr. Exhib. Proc., 2017: pp. 1– 7.

[17] M. Dios, Z. Gonzalez, P. Alvaredo, R. Bermejo, E. Gordo, B. Ferrari, Novel colloidal approach for the microstructural improvement in Ti(C,N)/FeNi cermets, J. Alloys Compd. 724 (2017) 327–338. doi:10.1016/j.jallcom.2017.07.034.

[18] I. Azkona, J.M. Sánchez, F. Castro, Effects of powder processing on densification of titanium diboride based cermets, Powder Metall. 47 (2004) 65–72. doi:10.1179/003258904225015527.

[19] Y. Zhao, Y. Zheng, W. Zhou, J. Zhang, Q. Huang, W. Xiong, Effect of carbon addition on the densification behavior, microstructure evolution and mechanical properties of

Ti(C, N)-based cermets, Ceram. Int. 42 (2016) 5487–5496. doi:10.1016/j.ceramint.2015.12.097.

[20]   P.K. Samal, J.W. Newkirk, ASM Handbook, Vol. 7, ASM International, 1998.

[21]   W.C. Oliver, G.M. Pharr, An improved technique for determining hardness and elastic modulus using load and displacement sensing indentation experiments, J. Mater. Res. 7 (1992) 1564–1580.

[22]   W.C. Oliver, G.M. Pharr, Measurement of hardness and elastic modulus by instrumented indentation: Advances in understanding and refinements to methodology, J. Mater. Res. 19 (2004) 3–20. doi:10.1117/12.461379.

[23]   G. Constantinides, F. Ulm, K. Van Vliet, On the use of nanoindentation for cementitious materials, Mater. Struct. 36 (2003) 191–196.

[24]   G. Constantinides, K.S. Ravi Chandran, F.J. Ulm, K.J. Van Vliet, Grid indentation analysis of composite microstructure and mechanics: Principles and validation, Mater. Sci. Eng. A. 430 (2006) 189–202. doi:10.1016/j.msea.2006.05.125.

[25]   G. Findenig, C. Buchegger, W. Lengauer, C. Veitsch, A. Demoly, Investigation of the main influencing parameters on the degassing behavior of titanium carbonitrides using mass spectrometry, Int. J. Refract. Met. Hard Mater. 63 (2017) 38–46. doi:10.1016/j.ijrmhm.2016.07.019.

[26]   W. Lengauer, F. Scagnetto, Ti(C,N)-Based Cermets: Critical Review of Achievements and Recent Developments, Solid State Phenom. 274 (2018) 53–100. doi:10.4028/www.scientific.net/SSP.274.53.

[27]   H. Besharatloo, M. de Nicolás, J.J. Roa, M. Dios, A. Mateo, B. Ferrari, E. Gordo, L. Llanes, Assessment of mechanical properties at microstructural length scale of Ti(C,N)–FeNi ceramic-metal composites by means of massive nanoindentation and statistical analysis, Ceram. Int. (2019). doi:10.1016/j.ceramint.2019.06.292.

[28]   J.P. Ramos, T. Stora, A.M.R. Senos, P. Bowen, Thermal stability of nanometric TiC-carbon composites: effects of carbon allotropes and Zr milling impurities, J. Eur. Ceram. Soc. 38 (2018) 4882–4891. doi:10.1016/j.jeurceramsoc.2018.07.002.

[29]   D.P. Xiang, Y. Liu, M.J. Tu, Y.Y. Li, W.P. Chen, Synthesis of nano Ti(C,N) powder by mechanical activation and subsequent carbothermal reduction-nitridation reaction, Int. J. Refract. Met. Hard Mater. 27 (2009). doi:doi:10.1016/j.ijrmhm.2008.04.006.

[30]   J. Zackrisson, H.-O. Andrén, Effect of carbon content on the microstructure and mechanical properties of (Ti, W, Ta, Mo)(C, N)-(Co, Ni) cermets, Int. J. Refract. Metals Hard Mater. 17 (1999) 265–273. doi:10.1016/S0263-4368(98)00074-2.

[31]   H. Besharatloo, M. de Nicolás, J.J. Roa, M. Dios, A. Mateo, B. Ferrari, E. Gordo, L. Llanes, Assessment of mechanical properties at microstructural length scale of Ti(C,N)–FeNi ceramic-metal composites by means of massive nanoindentation and statistical analysis, Ceram. Int. (2019). doi:10.1016/j.ceramint.2019.06.292.

[32]   J.J. Roa, E. Jiménez-Piqué, J.M. Tarragó, D.A. Sandoval, A. Mateo, J.Fair, L. Llanes, Hall-Petch strengthening of the constrained metallic binder in WC–Co cemented carbides: Experimental assessment by means of massive nanoindentation and statistical analysis, Mater. Sci. Eng. A. 676 (2016) 487–491. doi:10.1016/j.msea.2016.09.020.
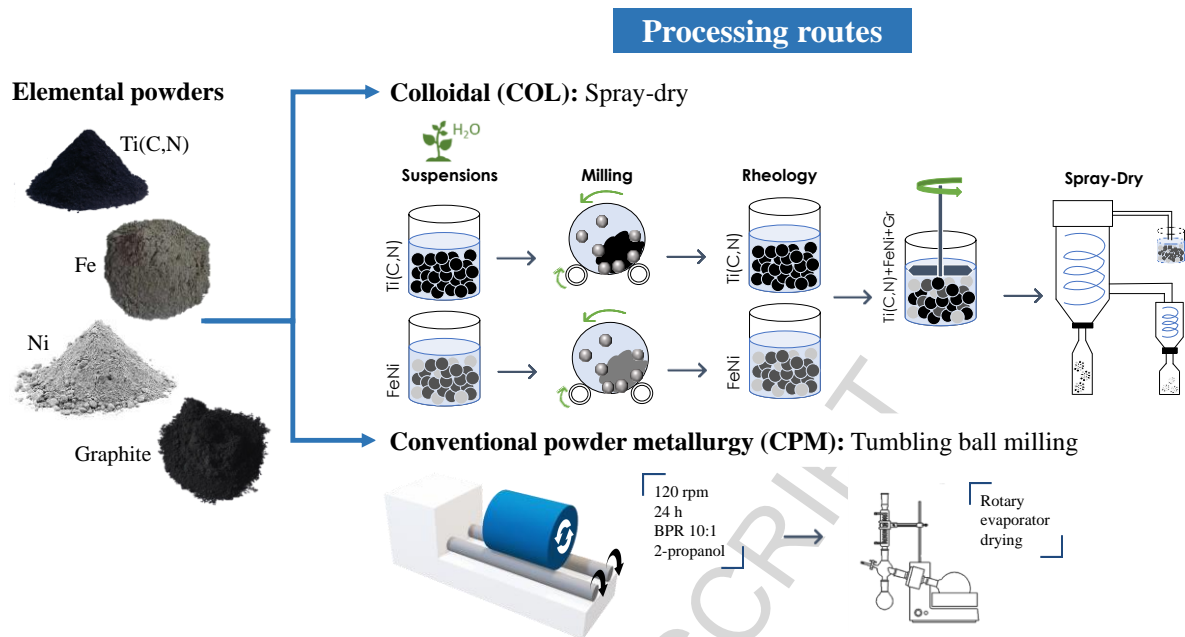
List of Figures

Figure 1. Schematic illustration of the two processing routes used in this investigation.
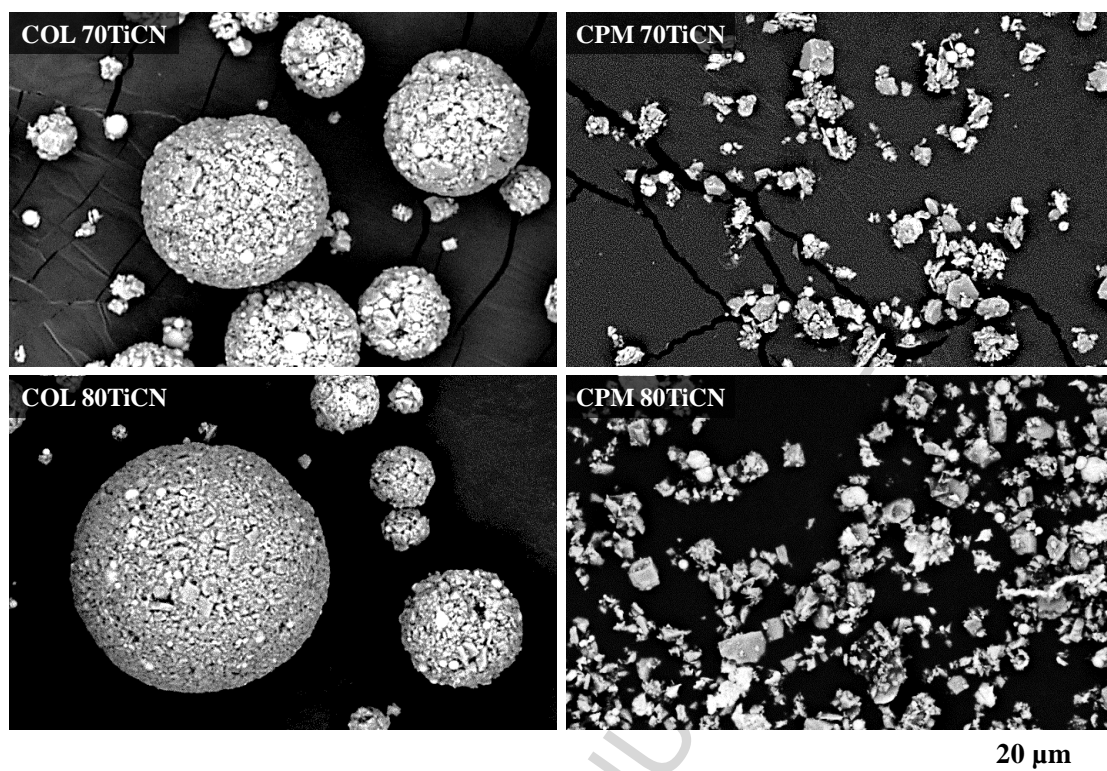
Figure 2. SEM micrographs (BSE mode) of the ceramic-metallic powder agglomerates for 70TiCN and 80TiCN compositions processed by CPM and COL techniques.

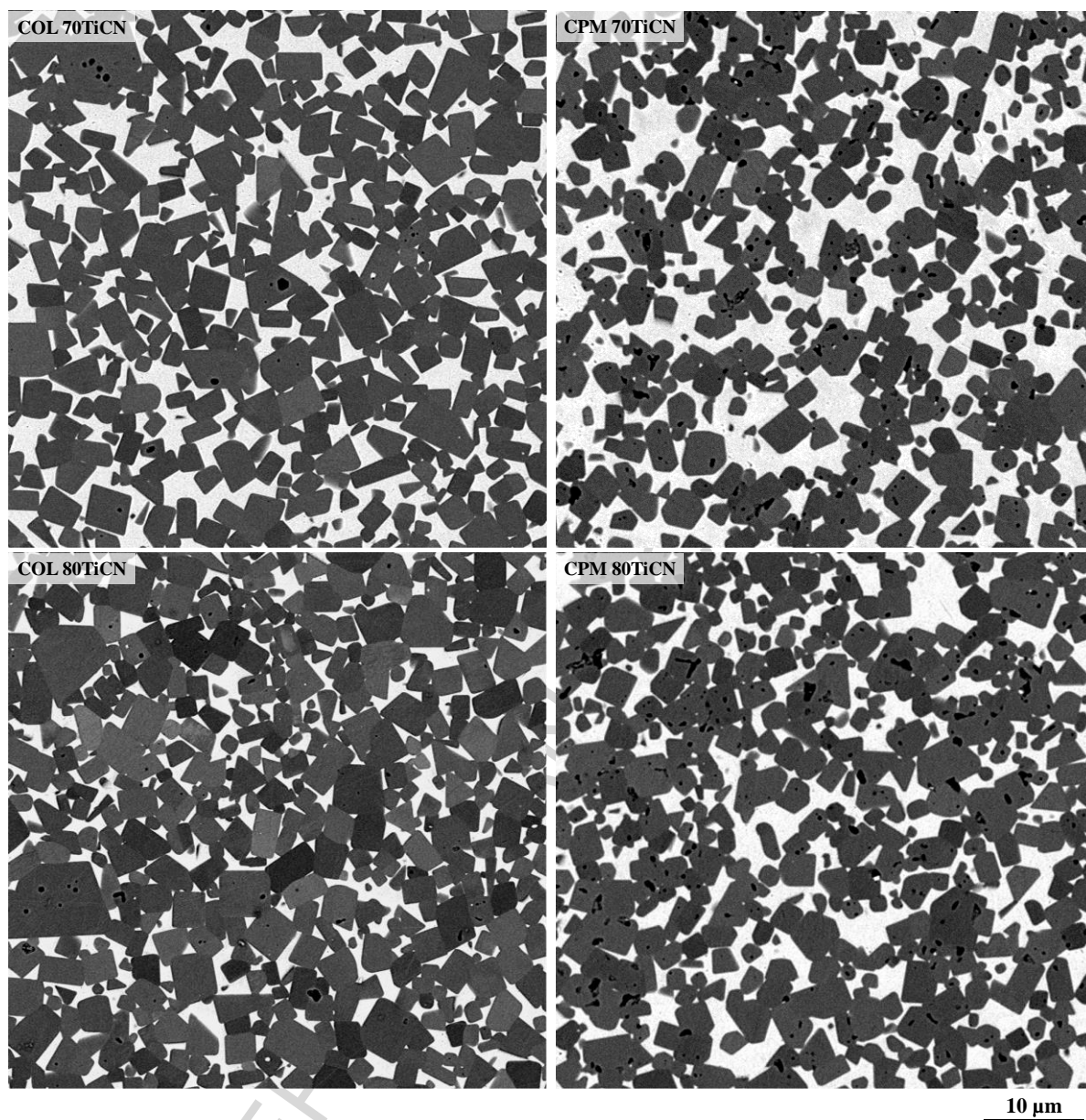**Figure 3.** SEM micrographs (BSE mode) of the sintered microstructures for 70TiCN and 80TiCN compositions processed using COL/CPM approaches.
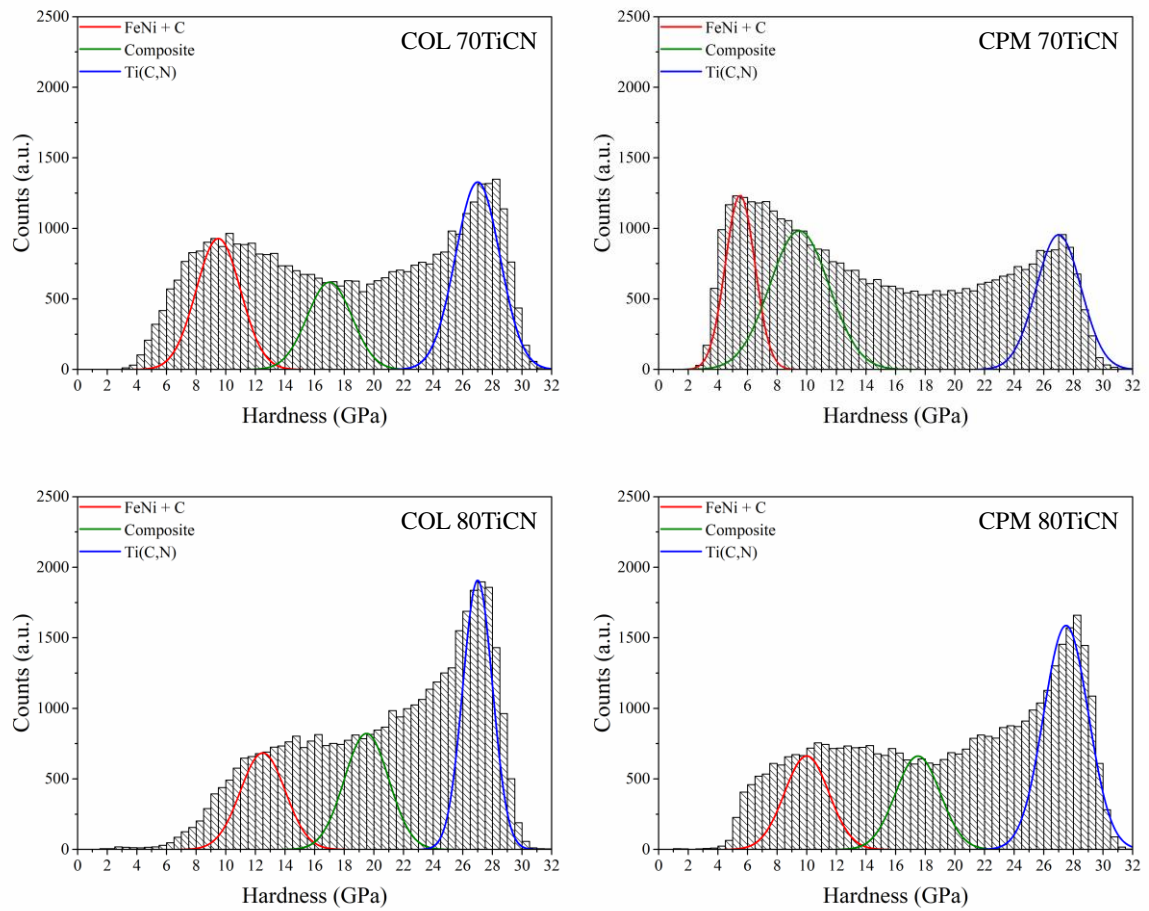
Figure 4. Massive nanoindentation histograms for 70TiCN and 80TiCN compositions.
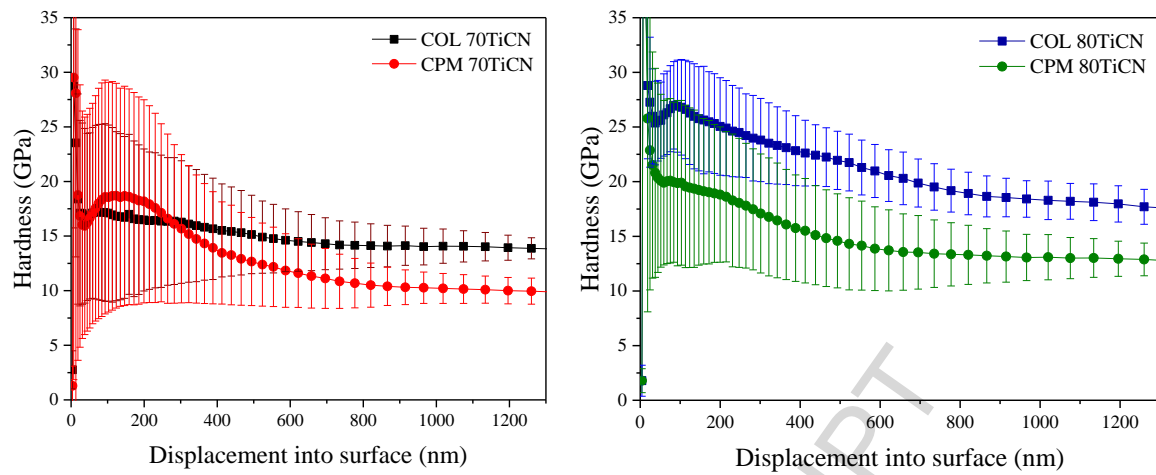
Figure 5. Composite Berkovich tests: nanoindenter composite hardness measurement (h~2000 nm) for 70TiCN (left) and 80TiCN (right) samples processed by COL and CPM routes.
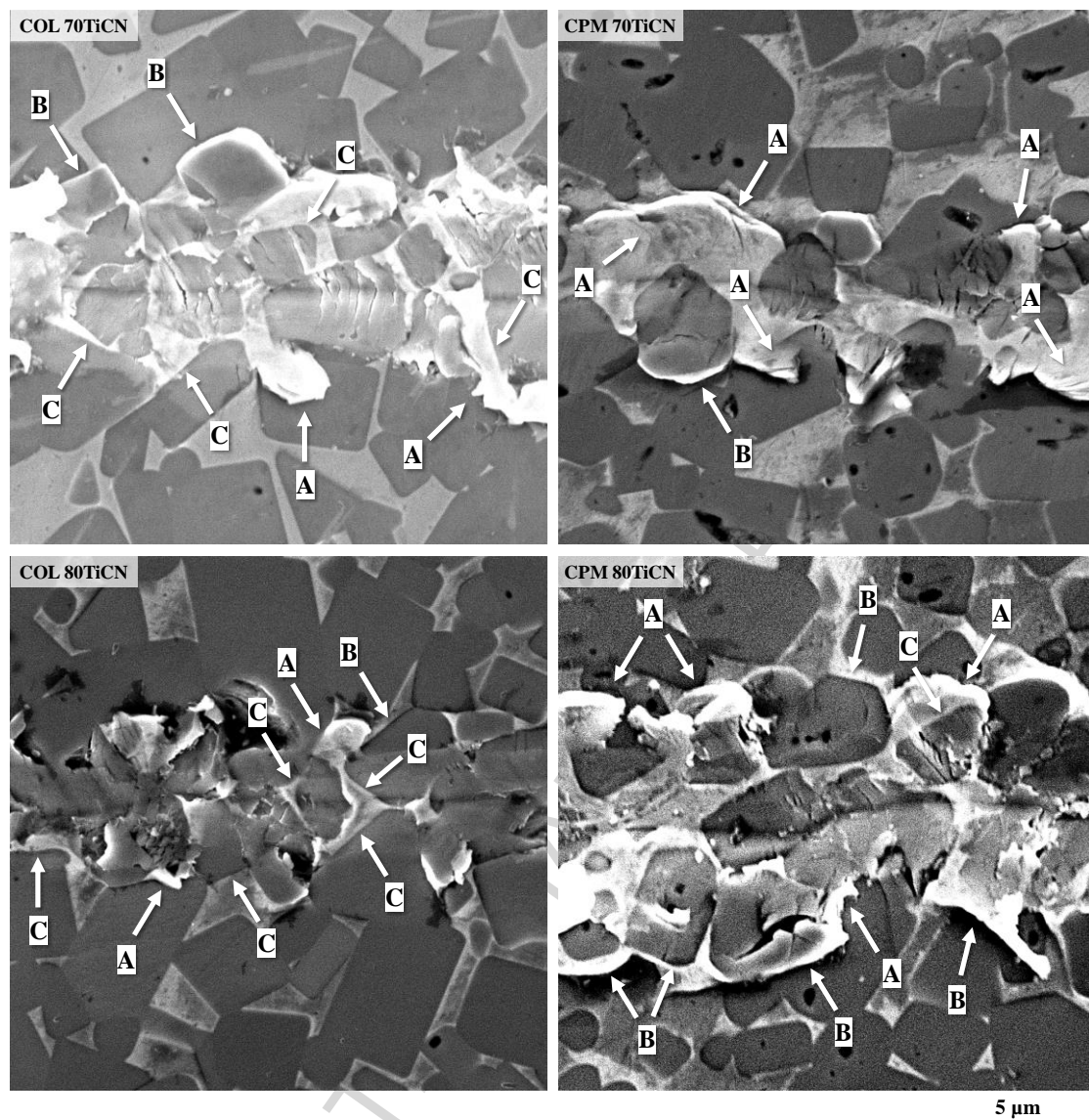
Figure 6. SEM images (BSE mode) of the nanoscratch tests performed on COL/CPM 70TiCN and 80TiCN samples. A, B and C labels point out binder ductile deformation, detachment and no-detachment at the ceramic-metal boundary, respectively.
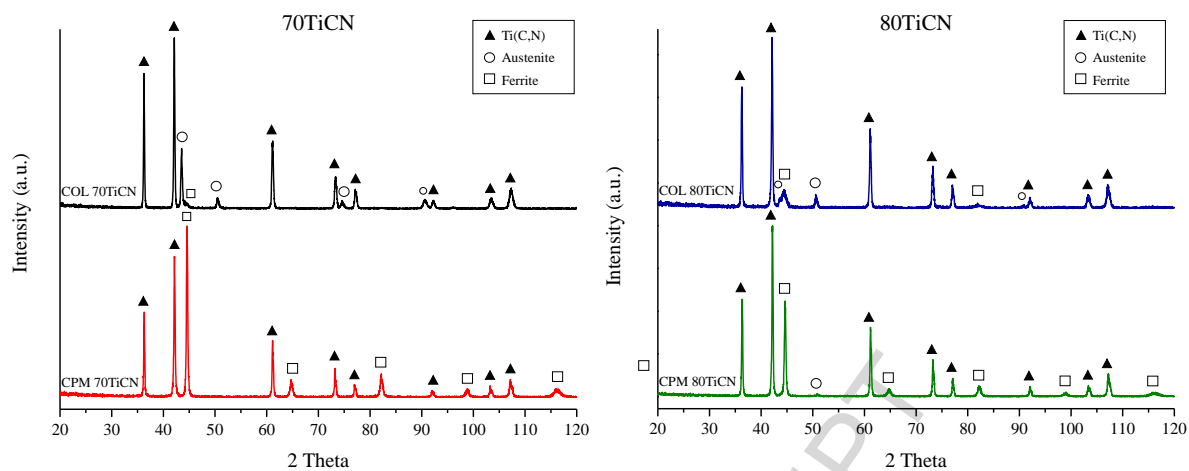
Figure 7. X-Ray diffractograms for 70TiCN (left) and 80TiCN (right) samples processed by COL (top)

and CPM (bottom) processing routes.

Table 1. **Summary of the two compositions investigated.**

Material name	Volume %		Equivalent cemented carbide grade [Co wt. %]
	Ceramic – Ti(C,N)	Metal – Fe15Ni	
70TiCN	70	30	20
80TiCN	80	20	12

Table 2. C measurements (LECO) for the processed powders and sintered samples of 70TiCN and 80TiCN COL/CPM materials.

Material	Processing route	C [wt. %]		
		Mixture powders	Sintered samples	C lost during sintering
70TiCN	COL	7.72 ± 0.04	6.85 ± 0.01	0.87
	CPM	6.45 ± 0.06	4.93 ± 0.18	1.52
	C difference	1.27	1.92	
80TiCN	COL	8.51 ± 0.01	7.75 ± 0.04	0.76
	CPM	7.35 ± 0.04	6.40 ± 0.04	0.95
	C difference	1.16	1.35	

Table 3. O content (LECO) of the powder mixtures for 70TiCN and 80TiCN COL/CPM materials.

Material	Processing route	Oxygen content of powder mixtures [O wt. %]
70TiCN	COL	1.95 ± 0.03
	CPM	2.41 ± 0.19
80TiCN	COL	1.69 ± 0.06
	CPM	2.23 ± 0.07

Table 4. Green/sintered relative densities and porosity percentages for 70TiCN and 80TiCN compositions processed by COL/CPM.

Material	Processing route	Green relative density [%]		Sintered relative density [%]			Porosity [%]		
		Geometric		Geometric	Pycnometric		Total porosity	Closed porosity	Open porosity
70TiCN	COL	67.3 ± 0.6		94.5 ± 0.5	98.5 ± 0.2		5.5 ± 0.5	1.5 ± 0.2	4.0 ± 0.5
	CPM	70.7 ± 0.9		95.7 ± 1.6	100.0 ± 0.9		4.3 ± 1.6	0.0 ± 0.9	4.3 ± 1.6
80TiCN	COL	65.7 ± 0.2		95.8 ± 0.9	97.8 ± 0.1		4.2 ± 0.9	2.2 ± 0.1	2.0 ± 0.9
	CPM	69.2 ± 0.3		96.8 ± 1.2	98.4 ± 0.2		3.2 ± 1.2	1.6 ± 0.2	1.6 ± 1.2

Table 5. Microstructure phase-quantification results, calculated by image analysis.

Theoretical FeNi vol. %	Theoretical Ti(C,N) vol. %	Processing route	Phase quantification of sintered samples [vol. %]			Mean free path, λ [μm]	Carbide diameter [μm]
			Binder phase	Ceramic phase	Error		
30	70	COL	24.2	75.8	1.2	0.96 ± 0.23	1.96 ± 1.14
		CPM	35.7	64.3	1.2	1.46 ± 1.34	1.74 ± 0.95
20	80	COL	16.7	83.3	1.4	0.56 ± 0.21	1.89 ± 1.05
		CPM	24.6	75.4	1.5	1.04 ± 0.93	1.85 ± 1.01

Table 6. Intrinsic (ceramic and binder) EDX analysis of the four studied materials, indicating the wt. % of the binder elements and at. % of the ceramic phase.

Element	Intrinsic (phase) EDX analysis							
	70-COL		70-CPM		80-COL		80-CPM	
	Ceramic (at. %)	Binder (wt. %)	Ceramic (at. %)	Binder (wt. %)	Ceramic (at. %)	Binder (wt. %)	Ceramic (at. %)	Binder (wt. %)
C	23.28±0.46	-	22.04±0.80	-	25.24±1.50	-	20.90±0.60	-
N	26.64±1.41	-	28.93±0.10	-	25.80±2.49	-	28.62±0.58	-
Ti	50.09±0.97	82.73±0.17	49.04±0.86	80.66±0.47	48.96±1.03	81.79±0.29	50.46±0.79	79.31±1.03
Fe	-	17.27±0.17	-	19.34±0.47	-	18.21±0.29	-	20.69±1.03
Ni	-		-		-		-	
Total	100	100	100	100	100	100	100	100
Fe/Ni ratio (theor.: 5.67)	-	4.79	-	4.17	-	4.49	-	3.83
C/N ratio (theor.: 1)	0.87	-	0.76	-	0.98	-	0.73	-
Ti/(C+N) ratio (theor.: 1)	1.00	-	0.96	-	0.96	-	1.02	-

Table 7. Intrinsic and composite hardness results for 70TiCN and 80TiCN COL/CPM samples. Colours in of the intrinsic hardness columns match the de-convoluted Gaussian curves of **Figure 4**.

Material	Processing route	Intrinsic hardness [GPa]		
		Binder	**Composite**	**Ti(C,N)**
70TiCN	COL	9.5 ± 0.1	16.5 ± 0.1	27 ± 2.0
	CPM	5.6 ± 0.1	9.6 ± 0.1	27 ± 2.0
80TiCN	COL	12.4 ± 0.1	19.5 ± 0.1	27 ± 2.0
	CPM	9.7 ± 0.1	17.4 ± 0.1	27 ± 2.0

Highlights

- Two routes were used for preparation of powders in the system Ti(C,N)-Fe15Ni: colloidal dispersion and wet milling
- The processing route directly affected the C content of the mixture powders
- A higher quantity of C in the final sintered materials favoured their density and mechanical integrity
- Small-scale hardness and sliding contact tests revealed influence of processing route on mechanical properties